COMMUNICATION

Photonic Crystals

ADVANCED
OPTICAL
MATERIALS

www.advopticalmat.de

Phototunable *Morpho* Butterfly Microstructures Modified by Liquid Crystal Polymers

Xin Qing, Yuyun Liu, Jia Wei, Ran Zheng, Chongyu Zhu, and Yanlei Yu*

The unique hierarchical microstructures of the *Morpho* butterfly wing (MBW) exhibit angle independent blue iridescence. Biomimicking these microstructures and turning them into functional photonic crystals (PhCs) have fascinated scientists yet remain challenging. Here, a phototunable PhC is fabricated by depositing the azobenzene-containing linear liquid crystal polymer (LLCP) onto the MBW template. Thanks to the excellent mechanical properties and deformability of LLCP, the generated 3D bilayer microstructures demonstrate hierarchical deformation upon UV light irradiation, leading to a blueshift of the reflection peak (70 nm) and a remarkable change of reflectance (40%). This phototunable PhC may have potential applications in pigments, cosmetics, and sensors.

Photonic crystals (PhCs) consist of periodic microstructures with a photonic bandgap[1] that prohibits light propagation at specific wavelength, endowing nature with brilliant reflective colors.[2] Manipulating the periodic structures to display variable colors is an effective strategy for communication, intimidation, and camouflage among creatures to survive the changeable environments.[3] Inspired by nature,[4] functional PhCs tuned by light,[5] temperature,[6] electricity,[7] stress,[8] and chemicals[9] have been developed and show great significance in controlling light for display, rewritable paper, sensors, telecommunication device, cloaking devices, and intelligent textiles.[3a,10] Techniques including lithography, layer-by-layer stacking, and self-assembly have allowed the fabrication of PhCs such as Bragg layers, opal and inverse opals; however, manufacture of more complicated natural PhC structures remains challenging.[2] Particularly, the hierarchical microstructured natural *Morpho* butterflies wing (MBW) with angle-independent blue iridescence has aroused many interests for the development of asymmetric wetting[11] materials, photocatalytic materials,[12] and responsive PhCs.[13] However, to fully reconstruct these

X. Qing, Dr. Y. Y. Liu, Dr. J. Wei, Dr. C. Y. Zhu, Prof. Y. L. Yu
Department of Materials Science
State Key Laboratory of Molecular Engineering of Polymers
Fudan University
220 Handan Road, Shanghai 200433, China
E-mail: ylyu@fudan.edu.cn
R. Zheng
Department of Chemistry
Fudan University
220 Handan Road, Shanghai 200433, China

The ORCID identification number(s) for the author(s) of this article can be found under https://doi.org/10.1002/adom.201801494.

fine structures (i.e., alternating layers of rectangle scales covered with the short-range periodic, multilayered ridges; details see Figure S1, Supporting Information)[14] with responsive materials will cost arduous effort.[15] In contrast, modification of MBW with responsive coatings directly inherits its delicate microstructures and the associated optical properties[14] while imparting a tunable reflection upon external stimuli. Such responsive coatings such as functional particles and hydrogels have demonstrated the potential to convert MBW into responsive photonic devices.[16]

In most reports, the reflection changes of MBW-based responsive PhCs were attributed to the deformation of their microstructures. However, due to the weak mechanical properties or deformability of the used coatings,[17] the deformation of MBW microstructures has not been observed, which limits the further understanding of the relationship between the deformation of microstructures and reflection change as well as controllable regulation of the reflectance of MBW-based responsive PhCs. Crosslinked liquid crystal polymer (CLCP), on the other hand, has excellent mechanical properties and deformability thanks to the combination of mesogen units and polymer networks.[18] The synergistic effect of aligned mesogens allows CLCP to amplify the nanoscopic molecular motions into huge macroscopic deformation[19] and to produce a force similar to that of muscle contraction.[20] The incorporation of photochromic moieties (e.g., azobenzene) into CLCP grants its response to light that enables localized, remote, and isothermal triggering and actuation.[21] Azobenzene-containing CLCP has been prepared into a variety of photoresponsive microstructures such as artificial cilia,[22] moving microrobots,[23] and dynamic surface patterns.[24] Therefore, CLCP is a promising candidate to serve as a responsive coating to induce significant deformation of MBW microstructures. However, their poor processing performance induced by the crosslinked chemical structures limits the fabrication of complex hierarchical microstructures.[25] Recently, our group has developed a novel azobenzene-containing linear liquid crystal polymer (LLCP), which possesses the photodeformability without chemical crosslinking, permitting the construction of more delicate 3D photoresponsive structures by commonly used solution and melting processing.[26]

Here, we report a new phototunable PhC by coating the azobenzene-containing LLCP onto MBW. Distinct from previous works on the elegant methods for modification of MBW, this work focuses on the deformation of the hierarchical microstructures. The LLCP was deposited onto the MBW surface

through electrospinning, which turned the LLCP solution into dry microscale fibers without altering the microstructures. A further melting and annealing process produced a well-orientated LLCP coating onto MBW to achieve a photoresponsive LLCP-MBW composite. The photoresponsiveness of the obtained composite was then studied, and for the first time, we observed the obvious deformation of the hierarchical microstructures of MBW including scales, ridges, and even lamella spacing upon low-energy UV light irradiation. Moreover, the detailed structure–reflection relationship was analyzed in this work to demonstrate that the deformation of hierarchical microstructures of LLCP-MBW could be adjusted by the light intensity, resulting in a large blueshift of the reflection peak and a tunable reflection intensity. It was noted that the change of reflectance could be restored by visible light and further repeated experiments have demonstrated a reliable reversibility of this bilayer composite, showing potentials in light sensors and chromic pigments.

The overall fabrication process of MBW-based phototunable PhC is illustrated **Figure 1**a, in which three tree-like ridges represent a piece of MBW. Instead of the conventional chemical

modification methods, electrospinning[27] was chosen as the polymer coating technology to avoid the use of solvent treatments or multi-step chemical treatments that might damage the microstructures of MBW. A 5 wt% LLCP solution in dichloromethane was optimized for uniform electrospinning onto the MBW surface without any pretreatment. The high number-average molecular weight (1.8×10^5 g mol^{-1}) and the non-crosslinked structure of LLCP enabled electrospinning to proceed smoothly. The microscale LLCP fibers were subsequently melted at 120 °C into a thin coating onto the microstructures. After annealing in liquid crystal (LC) phase at 55 °C for half an hour, the azobenzene mesogens were well orientated in the LLCP layer.[26]

Field emission scanning electron microscope (FESEM) was applied to investigate the topological change of the samples during the fabrication process. It was shown that the diameter of the obtained LLCP fibers through electrospinning was around 1 µm, which was close to the dimension of the MBW microstructure (Figure 1b medium). The morphology of LLCP-coated *Morpho* butterfly wing (LLCP-MBW, Figure 1b right) appeared similar to the original MBW (Figure 1b left) without
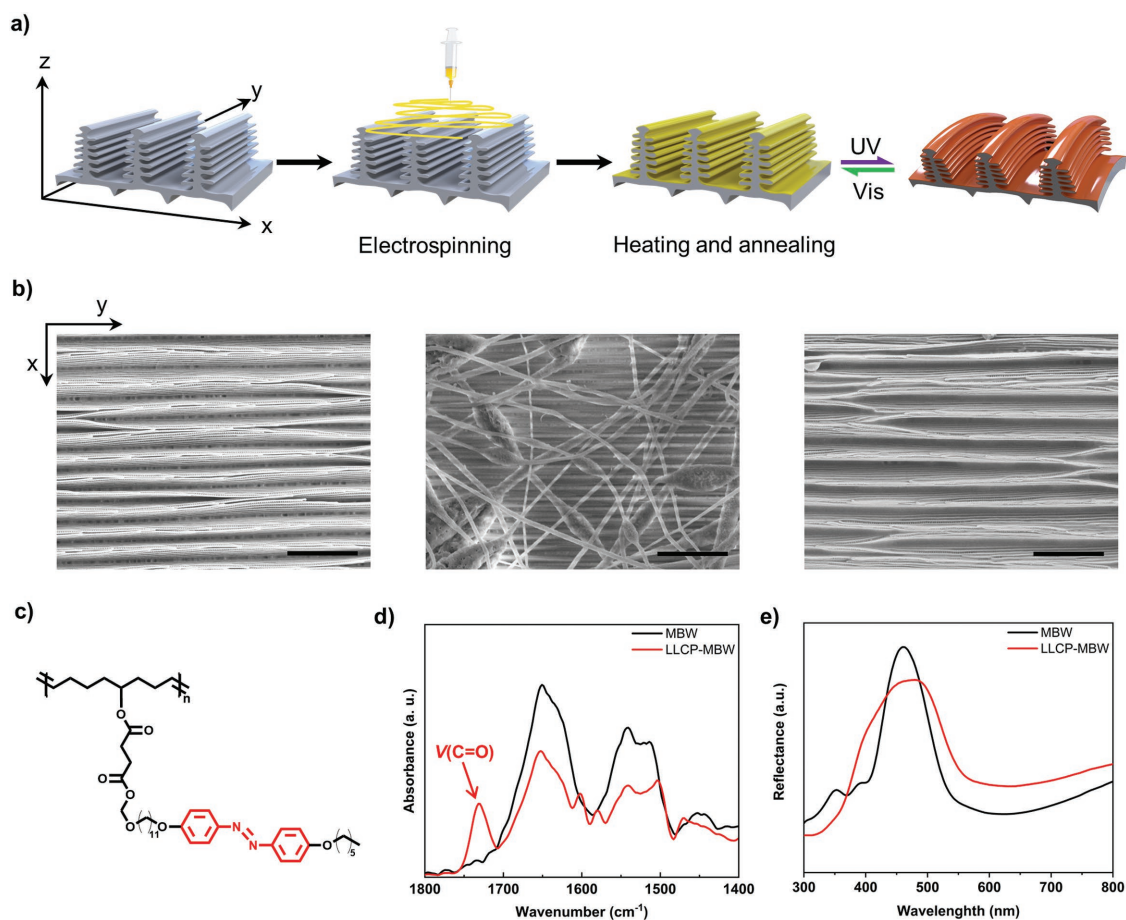

Figure 1. a) Schematic showing the fabrication of LLCP-coated *Morpho* butterfly wing (LLCP-MBW) and the reversible photoinduced deformation. For a better understanding of the placement of the MBW in this and the following figures, a coordinate system was set with *y*-axis parallel to the ridges, *x*-axis perpendicular to the ridges and *z*-axis vertical to the surface. b) SEM photos showing the top view of microstructures on MBW before electrospinning (left), after electrospinning (middle), and after heating and annealing (right). Scale bar, 5 µm. c) Chemical structure of the photoresponsive LLCP containing azobenzene mesogens. d) ATR-FTIR spectra of the MBW (black line) and LLCP-MBW (red line) in the region of 1800–1400 cm^{-1}. e) Reflective spectra of the MBW (black line) and LLCP-MBW (red line).

visible damage of the parallel-aligned ridges, proving that the microstructures were kept intact after modification. A further attenuated total reflectance Fourier transform infrared spectroscopy (ATR-FTIR) analysis was performed (Figure S2, Supporting Information). Compared to the absorbance of MBW, the new peak at 1730 cm^{-1} assigned to the −C=O stretching vibration of the carboxylic ester of LLCP was observed in LLCP-MBW (Figure 1d), elaborating the presence of the melted LLCP fibers on the surface of the photonic structures. Next, the influence of LLCP on the reflectance of MBW was analyzed by reflectance spectrometer (Figure 1e). The untreated MBW exhibited a strong reflection peak at 460 nm, while the LLCP-MBW showed a broader and a bit lower reflection peak shifted to 470 nm, suggesting a thin layer of LLCP on the surface of MBW slightly changed the effective refractive index.[28]

The photoresponsiveness of the LLCP-MBW was observed by the change of reflective spectra as shown in **Figure 2**a. After UV irradiation on LLCP-MBW for 10 s, the reflection peak at 470 nm decreased and a new peak at 397 nm appeared and increased following the variation of UV intensity from 10 mW cm^{-2} to 60 mW cm^{-2}, whereas the reflection change of uncoated MBW was trivial under the same treatment (Figure S3, Supporting Information). The reflection of LLCP-MBW recovered to the initial state upon 530 nm visible light irradiation (30 mW cm^{-2}, 10 s). Since the new reflection peak at 397 nm was not perceived by human eyes, the LLCP-MBW just reduced the brightness of blue iridescence upon UV irradiation

(Movie S1, Supporting Information). To quantify the changes in iridescence after UV exposures at different intensities, the concept of relative reflectance spectra ($R_r(\lambda)$)[16b] was introduced

$$R_r(\lambda) = \frac{R(\lambda)}{R_0(\lambda)} \times 100\% \tag{1}$$

where $R_0(\lambda)$ and $R(\lambda)$ were the reflectivity at λ before and after UV exposure, respectively. A 40% increase at 370 nm and a 35% decrease at 470 nm were observed in the reflection of LLCP-MBW, which were much larger than that of previous reports (typically less than 11%).[13a,16b]

The durability and stability of the LLCP coating were then studied by monitoring the reflectivity at 470 nm under alternating UV and visible light irradiation (Figure 2c). After each illumination during this process, the LLCP-MBW showed a reversible change for 50 cycles. The temperature of LLCP-MBW increased less than 3 °C (from 24.3 to 26.7 °C) during the whole process (Figure S4, Supporting Information), which was well below the clearing point of LLCP (90 °C),[26] indicating the change of reflectance was not attributed to the photothermal deformation of LLCP or MBW.

To study how the variation of reflectance was induced by the photodeformation of hierarchical structures on LLCP-MBW, the morphology change of the scales upon light irradiation was obtained by a super-resolution digital microscope. The blurred scale (out of focus) became clear (in focus) upon UV irradiation
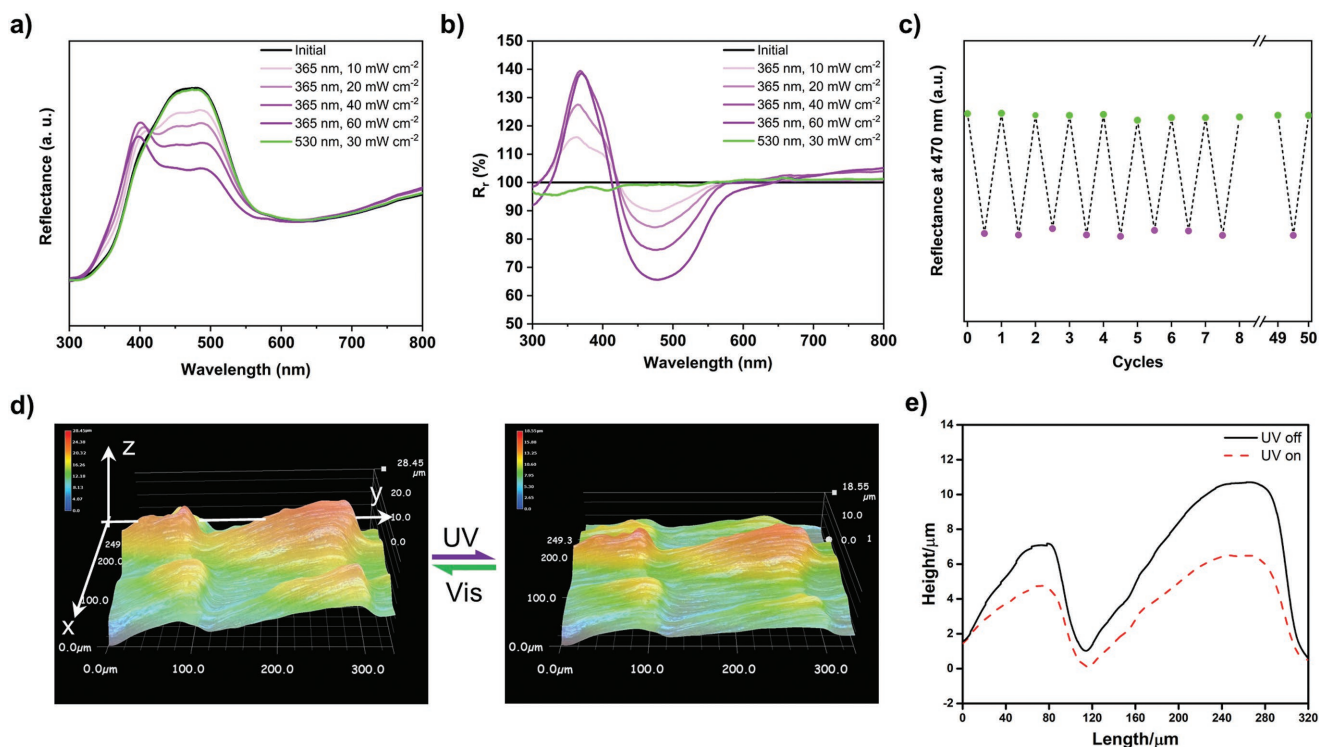

Figure 2. a–c) Reversible optical response of LLCP-MBW to UV and visible light irradiations. a) The changes of reflective spectra of LLCP-MBW after 365 nm UV irradiation with different intensities for 10 s and subsequent 530 nm visible light irradiation for 10 s. b) Relative reflectance (R_r) of LLCP-MBW shows the change ratio of reflection under different lights and intensities. c) Evaluation on the reversibility of LLCP-MBW in response to alternative irradiation of UV light (365 nm, 60 mW cm^{-2}, 10 s) and visible light (530 nm, 30 mW cm^{-2}, 10 s) for 50 cycles. d) 3D reconstruction images and e) surface profiles of the scales on the LLCP-MBW show the reversible deformation of the scales on LLCP-MBW upon UV (365 nm, 10 mW cm^{-2}) and visible light (white light from the microscope) irradiations. The deformation process is given in Movie S2 in the Supporting Information.

and was restored by the visible light source of the microscope after UV off, indicating the reversible height change of the scale (Movie S2, Supporting Information). To elucidate the subtle change, the 3D reconstruction of the scale was performed (Figure 2d). The surface profile of the 3D structures demonstrated that the tilted angle of the scales decreased with height dropped up to 4 µm upon UV irradiation in comparison to the original state (Figure 2e). The confocal microscopy suggested a similar movement of the scales on LLCP-MBW while no change was observed from the untreated MBW under UV irradiation, confirming that the deformation of the scales on LLCP-MBW was induced by the LLCP layer (Figure S5, Supporting Information).

To further demonstrate the microscale deformation on the LLCP-MBW scales, the in situ morphology change before and after UV irradiation was studied by atom force microscopy (AFM). Lines along and perpendicular the ridges were drawn between the ends of lamellas in the AFM photos to measure the deformation quantitatively, which demonstrated uneven shrinkage with average of 2.92% along the ridges and uneven expansion with average of 1.47% perpendicular to the ridges after UV irradiation. (Figure S6, Supporting Information) For example, as shown in **Figure 3**a, a line along the ridge shrank from 7.87 to 7.65 µm after UV irradiation, and the one perpendicular to the ridges expanded from 4.95 to 5.08 µm. Similar deformations were also observed by in situ FESEM (Figure 3b and Figure S7, Supporting Information). The AFM surface

profiles of LLCP-MBW before and after UV irradiation indicated a $(-6.9 \pm 1.3)\%$ height reduction of the ridges consisting of multiple lamellas (Figure S8, Supporting Information) and the maximum observed height decrease of a ridge was around 80 nm (Figure 3c).

According to the above experimental results, a mechanism for the deformation of the LLCP-MBW was proposed. To illustrate the deformation, a scale on LLCP-MBW was abstracted into a double-layered cuboid as shown in **Figure 4**a with ridges aligned along y-axis. The azobenzene mesogens were out-of-plane orientated in the LLCP layer according to the bending behavior of an LLCP film (Figure S9, Supporting Information).[26] Upon UV irradiation, the *trans–cis* isomerization of azobenzene mesogens decreased their length from 9.0 to 5.5 Å and disrupted the liquid crystal order, leading to the shrinkage of the LLCP layer thickness in z-axis and expansion in LLCP x–y plane. The in-plane expanded LLCP dragged the non-photoresponsive chitin MBW to bend along y-axis (the long side of the rectangular scale) away from the incident light,[29] thus the scales fixed to the substrate at one end exhibited a height reduction (Figure 4b). In smaller local areas, the microstructure on the scales showed only the expansion perpendicular to the ridges (x-axis), but "shrinkage" (actual expansion and bending) along the ridges (y-axis) due to the bending (Figure 4c). The shrinkage of LLCP layer in z-axis, on the other hand, reduced the thickness of the entire LLCP-MBW scale, resulting in contraction of the ridges thereon and decrease of lamella spacing.
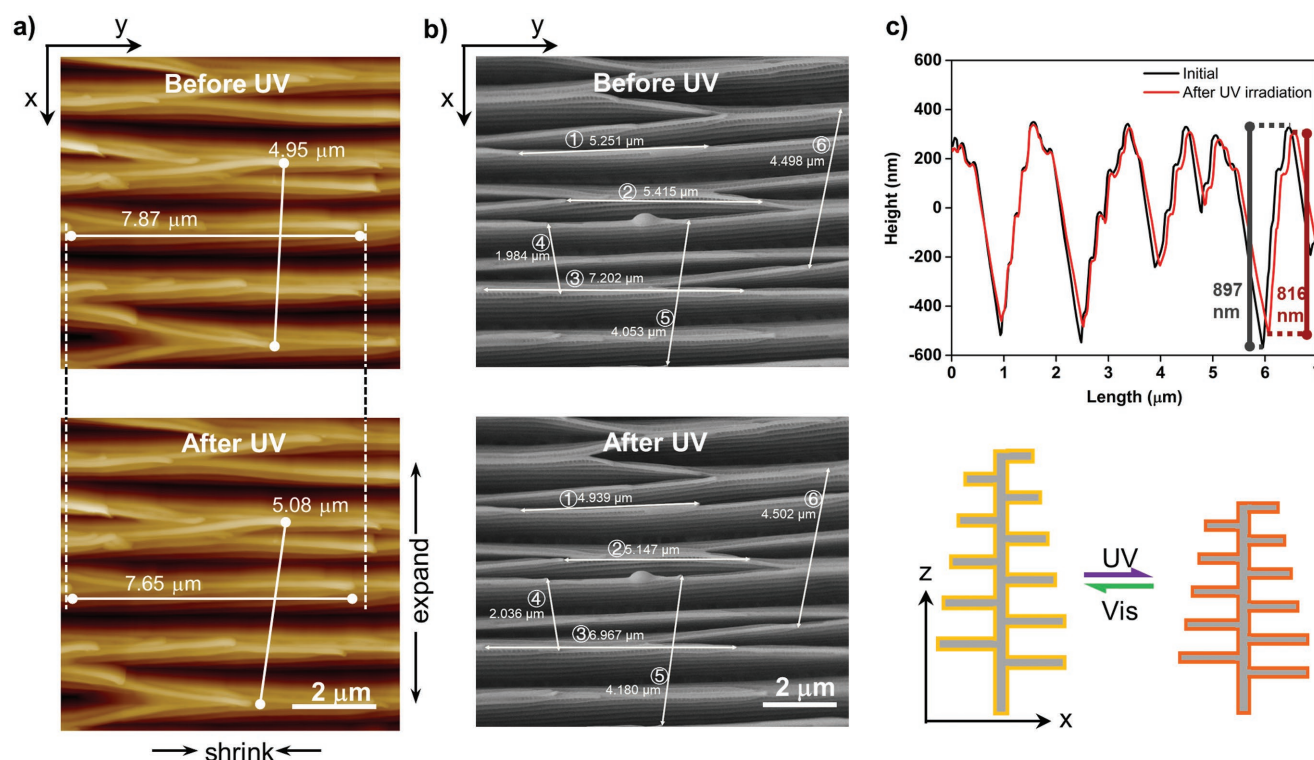

Figure 3. Photoinduced deformation of the microstructures on LLCP-MBW. a) In situ AFM images of the microstructures on the LLCP-MBW scales before and after UV irradiation. b) In situ FESEM images show the shrinkage along the ridges and the expansion perpendicular to the ridges according to the length changes of lines. c) Surface profiles of the microstructures before (black line) and after (red line) UV irradiation (upper) and schematic illustration of the expansion perpendicular to the ridges and shrinkage vertical to the ridges (lower). UV light: 365 nm, 10 mW cm^{-2}. The irradiation time was 10 s for AFM and 20 s for FESEM, respectively.
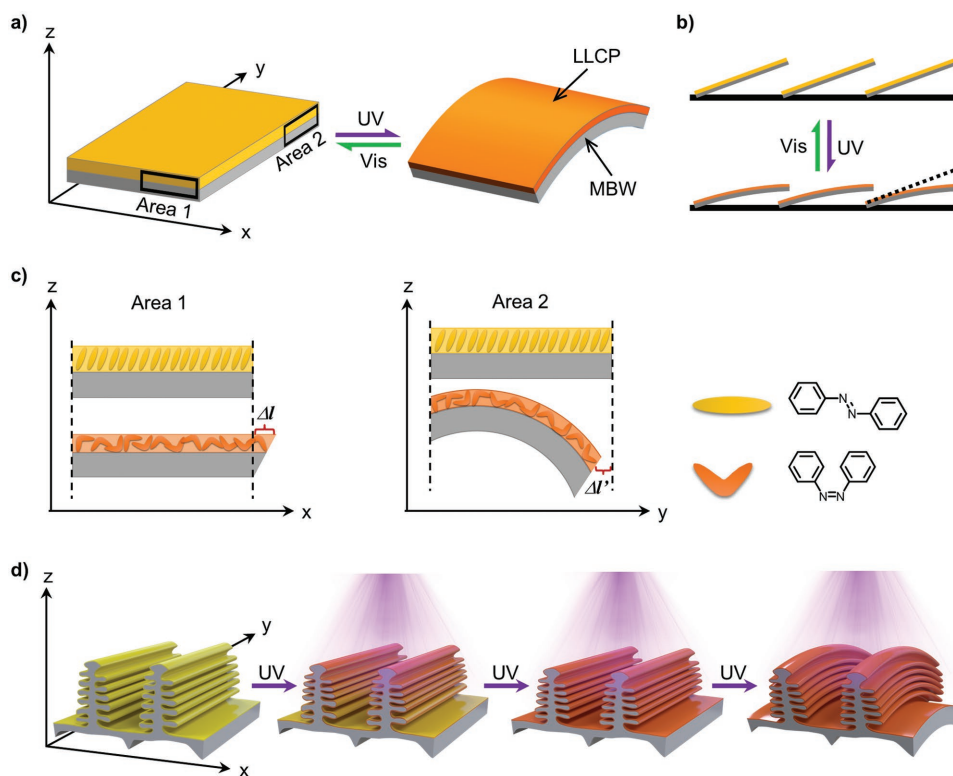
Figure 4. Schematic showing the deformation of the bilayer LLCP-MBW. a) A graphical representation of the scale on the LLCP-MBW abstracted into a two-layer cuboid where the yellow surface is the LLCP and the gray substrate is the MBW. Upon UV irradiation, the LLCP layer undergoes thickness decrease and in-plane expansion and drags the scale on MBW to bend away from the incident light. b) The tilted scales show height decrease owning to the bending deformation. c) Local deformation of the microstructures along x-axis (perpendicular to the ridges) and y-axis (along the ridges). d) With the increase of UV intensity, the penetration of incident light is gradually deepened in the lamellas of the ridges, causing the deformation of microstructures and the increasing of the new reflection peak at 397 nm gradually.

Having a better understanding of the deformation of LLCP-MBW, the mechanism of the reflection change was proposed. According to the Bragg equation,[28] the reduction of the lamella spacing and the decrease of LLCP layer thickness would induce a blueshift of the reflection peak. Owning to the high extinction coefficient of the *trans*-azobenzene at 365 nm,[30] only the top few layers of the lamella structures in LLCP-MBW absorbed the incident light and deformed into smaller layer spacing (Figure 4b), generating a new reflection peak at 397 nm. With the increase of light intensity, UV light penetrated deeper to deform the lower layers, enhancing the reflection intensity at 397 nm as shown in Figure 2.

In conclusion, we have demonstrated a new approach to fabricate phototunable PhCs with hierarchical microstructures by coating LLCP onto the natural MBW. Electrospinning coating technology was used here to directly deposit a thin layer of LLCP with high molecular weight on MBW, preserving the delicate photonic structures of MBW. Thanks to the excellent mechanical and deformable performance of LLCP, for the first time, we provided experimental evidences to show that the deformation of hierarchical microstructures could induce a reflection change of such MBW-based PhCs. In this work, obvious and reversible deformation of the hierarchical microstructures, including lamella spacing, ridges and the whole scales were observed from LLCP-MBW, which induced a blueshift of the reflection peak (70 nm) and a tunable reflection intensity (40%, three times larger than that of existing works) by UV light. This work sets up a moderate and effective strategy to combine the natural biotemplates and responsive LLCP to fabricate complex responsive microstructures. Furthermore, through a better understanding of the structure–reflection relationship of the MBW-based PhCs, we anticipate that the phototunable PhC will be used in a variety of applications ranging from sensors, photochromic pigments, anticounterfeiting to information storage technologies.

Experimental Section

General: The *Morpho* butterfly was supplied by Shanghai Dieyu Biological Technology Co., Ltd. The azobenzene-containing LLCP was synthesized according to the previous work.[19] 365 nm UV light was generated by an Omron ZUV-H30MC light source with a ZUV-C30H controller. 530 nm visible light was generated by a CCS HLV-24GR-3W light source with a PJ-1505-2CA controller. ATR-FTIR was measured on a Nicolet Nexus 470 spectrometer. The photothermal effects of UV light and visible light were recorded by a thermal imaging camera (FLIR, E40).

Fabrication of the LLCP-MBW: A concentration of 5 wt% of LLCP dichloromethane solution was used for electrospinning. The MBW was cut into pieces about 1 cm × 1 cm and placed on a metal basement to receive the polymer fibers. After electrospinning, the samples were heated to 120 °C (isotropic phase) on a hot stage (Mettler, FP-90 and

**ADVANCED
SCIENCE NEWS**

www.advancedsciencenews.com

**ADVANCED
OPTICAL
MATERIALS**

www.advopticalmat.de

FP-82) and then annealed at 55 °C (LC phase) for 30 min to obtain the LLCP-MBW.

Photoinduced Change of Reflectance: Reflective spectra were recorded on a reflection spectrometer (PG2000-Pro-EX, Ideaoptics Instruments) at room temperature. A standard white board (STD-WS, Ideaoptics Instruments) was used as the white reference. A 6 W tungsten-halogen light source (iDH2000-BSC, Ideaoptics Instruments) and a Y-shape optical fiber (FIB-S3-600TA-[..]-NIR fiber, Ideaoptics Instruments) with a reflection probe were used for the spectra collection. The probe was set to position that both the incident light and the reflected light were perpendicular to the sample surface. The LLCP-MBW and MBW were stuck to the glass sheet by black double-sided adhesive tapes for test. Measurements were performed before and after the sample was illuminated by UV light with intensity from 10 to 60 mW cm^{-2}. Then the sample was illuminated by green light at 30 mW cm^{-2} for 10 s and the reflective spectra was recorded again after the light off.

Photoinduced Deformation of the Scales: Movie S2 in the Supporting Information and the 3D reconstructed photos in Figure 2d were acquired by a super-resolution digital microscope (Keyence, VHX-1000C). The photodeformation of the scales was achieved by the in situ UV irradiation of 10 mW cm^{-2} and the restoration was performed upon the white light from the lens of microscope. Surface profiles in Figure 2e, Figure S5 and simulated morphology in Figure S5 in the Supporting Information were acquired by a confocal microscopy (Leica, DCM8). All measurements were performed in the same location to verify the change in the surface topography. The deformation measurements were conducted before and after the illumination upon UV light with the intensity from 5 to 15 mW cm^{-2} for 10 s. The restoration of deformation were measured after the green light (10 mW cm^{-2}) illumination for 20 s.

Photoinduced Deformation of the Microstructures: The morphology of microstructures before and after UV irradiation (10 mW cm^{-2}) was acquired in situ by an atomic force microscope (AFM, Bruker, Dimension Edge) in tapping mode and a field emission scanning electron microscope (FESEM, Zeiss, Ultra 55 and Zeiss, Sigma) at an accelerating voltage of 3 kV. The irradiation time was 10 s for AFM and 20 s for FESEM, respectively.

Supporting Information

Supporting Information is available from the Wiley Online Library or from the author.

Conflict of Interest

The authors declare no conflict of interest.

[1] Y. J. Zhao, Z. Y. Xie, H. C. Gu, C. Zhu, Z. Z. Gu, *Chem. Soc. Rev.* **2012**, *41*, 3297.

[2] A. G. Dumanli, T. Savin, *Chem. Soc. Rev.* **2016**, *45*, 6698.

[3] a) G. Isapour, M. Lattuada, *Adv. Mater.* **2018**, *30*, 1707069; b) M. Vatankhah-Varnosfaderani, A. N. Keith, Y. D. Cong, H. Y. Liang, M. Rosenthal, M. Sztucki, C. Clair, S. Magonov, D. A. Ivanov, A. V. Dobrynin, S. S. Sheiko, *Science* **2018**, *359*, 1509; c) D. Gur, B. A. Palmer, B. Leshem, D. Oron, P. Fratzl, S. Weiner, L. Addadi, *Angew. Chem., Int. Ed.* **2015**, *54*, 12426; d) E. Moyroud, T. Wenzel, R. Middleton, P. J. Rudall, H. Banks, A. Reed, G. Mellers, P. Killoran, M. M. Westwood, U. Steiner, S. Vignolini, B. J. Glover, *Nature* **2017**, *550*, 469.

[4] a) L. P. Wu, J. Q. He, W. Shang, T. Deng, J. J. Gu, H. L. Su, Q. L. Liu, W. Zhang, D. Zhang, *Adv. Opt. Mater.* **2016**, *4*, 195; b) E. Goi, B. P. Cumming, M. Gu, *Adv. Opt. Mater.* **2018**, *6*, 1800485; c) E. S. Goerlitzer, R. N. Klupp Taylor, N. Vogel, *Adv. Mater.* **2018**, *30*, 1706654.

[5] a) L. Qin, W. Gu, J. Wei, Y. L. Yu, *Adv. Mater.* **2018**, *30*, 1704941; b) H. K. Bisoyi, Q. Li, *Chem. Rev.* **2016**, *116*, 15089.

[6] a) A. J. J. Kragt, D. J. Broer, A. P. H. J. Schenning, *Adv. Funct. Mater.* **2018**, *28*, 1704756; b) Y. Ohtsuka, T. Seki, Y. Takeoka, *Angew. Chem., Int. Ed.* **2015**, *54*, 15368; c) M. Chen, Y. P. Zhang, S. Y. Jia, L. Zhou, Y. Guan, Y. J. Zhang, *Angew. Chem., Int. Ed.* **2015**, *54*, 9257; d) Z. Zhao, H. Wang, L. Shang, Y. Yu, F. Fu, Y. Zhao, Z. Gu, *Adv. Mater.* **2017**, *29*, 1704569.

[7] a) M. Wang, C. Zou, J. Sun, L. Y. Zhang, L. Wang, J. M. Xiao, F. S. Li, P. Song, H. Yang, *Adv. Funct. Mater.* **2017**, *27*, 1702261; b) H. K. Chang, J. Park, *Adv. Opt. Mater.* **2018**, *6*, 1800792.

[8] a) D. Ge, E. Lee, L. Yang, Y. Cho, M. Li, D. S. Gianola, S. Yang, *Adv. Mater.* **2015**, *27*, 2489; b) F. Fu, L. Shang, Z. Chen, Y. Yu, Y. Zhao, *Sci. Rob.* **2018**, *3*, eaar8580; c) C. Pouya, J. T. Overvelde, M. Kolle, J. Aizenberg, K. Bertoldi, J. C. Weaver, P. Vukusic, *Adv. Opt. Mater.* **2016**, *4*, 99.

[9] a) J. P. Couturier, M. Sutterlin, A. Laschewsky, C. Hettrich, E. Wischerhoff, *Angew. Chem., Int. Ed.* **2015**, *54*, 6641; b) M. Moirangthem, R. Arts, M. Merkx, A. P. H. J. Schenning, *Adv. Funct. Mater.* **2016**, *26*, 1154; c) K. Szendrei-Temesi, O. Sanchez-Sobrado, S. B. Betzler, K. M. Durner, T. Holzmann, B. V. Lotsch, *Adv. Funct. Mater.* **2018**, *28*, 1705740; d) Y. Fang, Y. L. Ni, B. Choi, S. Y. Leo, J. Gao, B. Ge, C. Taylor, V. Basile, P. Jiang, *Adv. Mater.* **2015**, *27*, 3696; e) M. Giese, L. K. Blusch, M. K. Khan, M. J. MacLachlan, *Angew. Chem., Int. Ed.* **2015**, *54*, 2888; f) M. Qin, M. Sun, R. Bai, Y. Mao, X. Qian, D. Sikka, Y. Zhao, H. J. Qi, Z. Suo, X. He, *Adv. Mater.* **2018**, *30*, 1800468.

[10] M. I. Khazi, W. Jeong, J. M. Kim, *Adv. Mater.* **2018**, *30*, 1705310.

[11] a) C. C. Liu, J. Ju, Y. M. Zheng, L. Jiang, *ACS Nano* **2014**, *8*, 1321; b) Z. W. Hang, Z. Z. Mu, B. Li, Z. Wang, J. Q. Zhang, S. C. Niu, L. Q. Ren, *ACS Nano* **2016**, *10*, 8591.

[12] a) M. Chen, J. J. Gu, C. Sun, Y. X. Zhao, R. X. Zhang, X. Y. You, Q. L. Liu, W. Zhang, Y. S. Su, H. L. Su, D. Zhang, *ACS Nano* **2016**, *10*, 6693; b) R. E. Rodriguez, S. P. Agarwal, S. An, E. Kazyak, D. Das, W. Shang, R. Skye, T. Deng, N. P. Dasgupta, *ACS Appl. Mater. Interfaces* **2018**, *10*, 4614; c) J. Fang, J. J. Gu, Q. L. Liu, W. Zhang, H. L. Su, D. Zhang, *ACS Appl. Mater. Interfaces* **2018**, *10*, 19649; d) S. Lou, X. M. Guo, T. X. Fan, D. Zhang, *Energy Environ. Sci.* **2012**, *5*, 9195.

[13] a) R. A. Potyrailo, T. A. Starkey, P. Vukusic, H. Ghiradella, M. Vasudev, T. Bunning, R. R. Naik, Z. X. Tang, M. Larsen, T. Deng, S. Zhong, M. Palacios, J. C. Grande, G. Zorn, G. Goddard, S. Zalubovsky, *Proc. Natl. Acad. Sci. USA* **2013**, *110*, 15567; b) Y. Mohri, J. Kobashi, H. Yoshida, M. Ozaki, *Adv. Opt. Mater.* **2017**, *5*, 1601071; c) X. Fei, T. Lu, J. Ma, S. Zhu, D. Zhang, *Nanoscale* **2017**, *9*, 12969.

[14] a) S. Kinoshita, S. Yoshioka, K. Kawagoe, *Proc. R. Soc. B* **2002**, *269*, 1417; b) K. Chung, S. Yu, C. J. Heo, J. W. Shim, S. M. Yang, M. G. Han, H. S. Lee, Y. Jin, S. Y. Lee, N. Park, J. H. Shin, *Adv.*

**ADVANCED
SCIENCE NEWS**

www.advancedsciencenews.com

**ADVANCED
OPTICAL
MATERIALS**

www.advopticalmat.de

Mater. **2012**, *24*, 2375; c) Q. Shen, J. He, M. Ni, C. Song, L. Zhou, H. Hu, R. Zhang, Z. Luo, G. Wang, P. Tao, *Small* **2015**, *11*, 5705.

[15] a) G. Zyla, A. Kovalev, M. Grafen, E. L. Gurevich, C. Esen, A. Ostendorf, S. Gorb, *Sci. Rep.* **2017**, *7*, 17622; b) B. Song, V. E. Johansen, O. Sigmund, J. H. Shin, *Sci. Rep.* **2017**, *7*, 46023; c) S. Zhang, Y. Chen, B. Lu, J. Liu, J. Shao, C. Xu, *Nanoscale* **2016**, *8*, 9118; d) C. A. Tippets, Y. L. Fu, A. M. Jackson, E. U. Donev, R. Lopez, *J. Opt.* **2016**, *18*, 065105.

[16] a) A. D. Pris, Y. Utturkar, C. Surman, W. G. Morris, A. Vert, S. Zalyubovskiy, T. Deng, H. T. Ghiradella, R. A. Potyrailo, *Nat. Photonics* **2012**, *6*, 564; b) F. Y. Zhang, Q. C. Shen, X. D. Shi, S. P. Li, W. L. Wang, Z. Luo, G. F. He, P. Zhang, P. Tao, C. Y. Song, W. Zhang, D. Zhang, T. Deng, W. Shang, *Adv. Mater.* **2015**, *27*, 1077; c) W. H. Peng, S. M. Zhu, W. L. Wang, W. Zhang, J. J. Gu, X. B. Hu, D. Zhang, Z. X. Chen, *Adv. Funct. Mater.* **2012**, *22*, 2072; d) Q. C. Shen, Z. Luo, S. Ma, P. Tao, C. Y. Song, J. B. Wu, W. Shang, T. Deng, *Adv. Mater.* **2018**, *30*, 1707632.

[17] a) Q. Q. Yang, S. M. Zhu, W. H. Peng, C. Yin, W. L. Wang, J. J. Gu, W. Zhang, J. Ma, T. Deng, C. L. Feng, D. Zhang, *ACS Nano* **2013**, *7*, 4911; b) D. D. Xu, H. A. Yu, Q. Xu, G. H. Xu, K. X. Wang, *ACS Appl. Mater. Interfaces* **2015**, *7*, 8750; c) W. H. Peng, S. M. Zhu, W. Zhang, Q. Q. Yang, D. Zhang, Z. X. Chen, *Nanoscale* **2014**, *6*, 6133.

[18] a) C. Ohm, M. Brehmer, R. Zentel, *Adv. Mater.* **2010**, *22*, 3366; b) Y. L. Yu, T. Ikeda, *Angew. Chem., Int. Ed.* **2006**, *45*, 5416.

[19] a) A. H. Gelebart, D. J. Mulder, M. Varga, A. Konya, G. Vantomme, E. Meijer, R. L. Selinger, D. J. Broer, *Nature* **2017**, *546*, 632; b) W. Feng, D. J. Broer, D. Q. Liu, *Adv. Mater.* **2018**, *30*, 1704970; c) T. H. Ware, M. E. McConney, J. J. Wie, V. P. Tondiglia, T. J. White, *Science* **2015**, *347*, 982; d) Z. Q. Pei, Y. Yang, Q. M. Chen, E. M. Terentjev, Y. Wei, Y. Ji, *Nat. Mater.* **2014**, *13*, 36; e) O. M. Wani, H. Zeng, A. Priimagi, *Nat. Commun.* **2017**, *8*, 15546; f) X. Y. Liu, R. B. Wei, P. T. Hoang, X. G. Wang, T. Liu, P. Keller, *Adv. Funct.*

Mater. **2015**, *25*, 3022; g) S. Iamsaard, S. J. Asshoff, B. Matt, T. Kudernac, J. J. L. M. Cornelissen, S. P. Fletcher, N. Katsonis, *Nat. Chem.* **2014**, *6*, 229; h) Y. Y. Liu, B. Xu, S. T. Sun, J. Wei, L. M. Wu, Y. L. Yu, *Adv. Mater.* **2017**, *29*, 1604792; i) R. Yang, Y. Zhao, *Angew. Chem., Int. Ed.* **2017**, *56*, 14202; j) Y. Xia, X. Y. Zhang, S. Yang, *Angew. Chem., Int. Ed.* **2018**, *57*, 5665.

[20] a) X. Qing, L. Qin, W. Gu, Y. Yu, *Liq. Cryst.* **2016**, *43*, 2114; b) T. J. White, D. J. Broer, *Nat. Mater.* **2015**, *14*, 1087; c) D. L. Thomsen, P. Keller, J. Naciri, R. Pink, H. Jeon, D. Shenoy, B. R. Ratna, *Macromolecules* **2001**, *34*, 5868.

[21] T. Ube, T. Ikeda, *Angew. Chem., Int. Ed.* **2014**, *53*, 10290.

[22] C. L. van Oosten, C. W. M. Bastiaansen, D. J. Broer, *Nat. Mater.* **2009**, *8*, 677.

[23] a) H. Zeng, P. Wasylczyk, C. Parmeggiani, D. Martella, M. Burresi, D. S. Wiersma, *Adv. Mater.* **2015**, *27*, 3883; b) S. Palagi, A. G. Mark, S. Y. Reigh, K. Melde, T. Qiu, H. Zeng, C. Parmeggiani, D. Martella, A. Sanchez-Castillo, N. Kapernaum, F. Giesselmann, D. S. Wiersma, E. Lauga, P. Fischer, *Nat. Mater.* **2016**, *15*, 647.

[24] a) D. Q. Liu, C. W. M. Bastiaansen, J. M. J. den Toonder, D. J. Broer, *Angew. Chem., Int. Ed.* **2012**, *51*, 892; b) D. Q. Liu, L. Liu, P. R. Onck, D. J. Broer, *Proc. Natl. Acad. Sci. USA* **2015**, *112*, 3880; c) Y. Zhan, J. Zhao, W. Liu, B. Yang, J. Wei, Y. Yu, *ACS Appl. Mater. Interfaces* **2015**, *7*, 25522; d) C. Li, F. T. Cheng, J. A. Lv, Y. Zhao, M. J. Liu, L. Jiang, Y. L. Yu, *Soft Matter* **2012**, *8*, 3730.

[25] X. Qing, J. A. Lv, Y. L. Yu, *Acta Polym. Sin.* **2017**, *11*, 1679.

[26] J. A. Lv, Y. Y. Liu, J. Wei, E. Q. Chen, L. Qin, Y. L. Yu, *Nature* **2016**, *537*, 179.

[27] J. Wu, N. Wang, Y. Zhao, L. Jiang, *J. Mater. Chem. A* **2013**, *1*, 7290.

[28] C. Fenzl, T. Hirsch, O. S. Wolfbeis, *Angew. Chem., Int. Ed.* **2014**, *53*, 3318.

[29] M. Kondo, Y. L. Yu, T. Ikeda, *Angew. Chem., Int. Ed.* **2006**, *45*, 1378.

[30] H. F. Yu, T. Ikeda, *Adv. Mater.* **2011**, *23*, 2149.